Efficient Light Harvesting by Photon Downconversion and Light Trapping in Hybrid ZnS Nanoparticles/Si Nanotips Solar Cells

Chun-Ying Huang,[†] Di-Yan Wang,[§] Chun-Hsiung Wang,[‡] Yung-Ting Chen,[‡] Yaw-Tyng Wang,[§] You-Ting Jiang,[§] Ying-Jay Yang,[†] Chia-Chun Chen,[§,⊥] and Yang-Fang Chen[‡,*]

[†]Graduate Institute of Electronics Engineering and [‡]Department of Physics, National Taiwan University, Taipei 106, Taiwan, [§]Department of Chemistry, National Taiwan Normal University, Taipei, 116, Taiwan, and [⊥]Institute of Atomic and Molecular Sciences, Academia Sinica, Taipei, 106, Taiwan

ABSTRACT A hybrid colloidal ZnS nanoparticles/Si nanotips p—n active layer has been demonstrated to have promising potential for efficient solar spectrum utilization in crystalline silicon-based solar cells. The hybrid solar cell shows an enhancement of 20% in the short-circuit current and approximately 10% in power conversion efficiency compared to its counterpart without integrating ZnS nanoparticles. The enhancement has been investigated by external quantum efficiency, photoluminescence excitation spectrum, photoluminescence, and reflectance to distinct the role of ZnS quantum dots for light harvesting. It is concluded that ZnS nanoparticles not only act as frequency downconversion centers in the ultraviolet region but also serve as antireflection coating for light trapping in the measured spectral regime. Our approach is ready to be extended to many other material systems for the creation of highly efficient photovoltaic devices.

KEYWORDS: solar cell · downconversion · light trapping · quantum dot · silicon nanotips · light harvesting

At present, single and multicrystalline silicon (Si) solar cells have been the workhorse for this market, taking over 80% of total cell production, due to their advantages of availability and mature of processing. With the progress of the semiconductor industry, Si is not only much purer than metallurgical grade but it is also in single-crystal form with a very small amount of defects for solar cell application. Moreover, Si is the second most abundant element in the earth's crust compared to poisonous or rare elements used as solar cell materials, for example, GaAs, CdTe, and CuInGaSe (CIGS).[1−4]

Despite the above-mentioned superiority in the solar cell field, Si solar cells still suffer from many challenges to reach high efficiency. There are four main losses that reduce the conversion efficiency of Si solar cells: (1) optical; (2) recombination; (3) series resistance; and (4) thermal or quantum losses.[1,2] For the improvement of cell efficiency, recently, research into the use of subwavelength structures, such as nanowires or nanotips, has received a significant interest.[5,6] It is well-known that polished substrates reflect approximately 30−35% of incident photons. By contrast, subwavelength structures on the front side of solar cell surface reflect only <10% of the incident photons. This strategy significantly reduces optical losses and thereby increases the short-circuit current (Jsc). In addition, optical losses of the air−semiconductor interface can also be reduced using an antireflection coating. An antireflection coating is a continuous thin film with refractive index intermediate between those of semiconductor (n_s) and air (n_0).[1−4] For example, SiO_2 (n = 1.5),[7] Si_3N_4 (n = 2.0),[8,9] Ta_2O_5 (n = 2.25),[10,11] TiO_2 (n = 2.3),[7] Al_2O_3 (n = 1.85),[10] and MgF_2 (n = 1.38)[10] have been reported to be the prime elements for antireflection coating thus far. More importantly, the major part of the energy losses (~52%) is related to the spectral mismatch, known as thermal or quantum losses. A large part of high-energy photons is lost as heat through phonon scattering, resulting in the limitation of power conversion efficiency of Si solar cells. The ultraviolet (UV) part of the solar spectrum (about 7% of the entire solar spectrum) cannot efficiently be used by Si solar cells. During the past decade, many rare earth-doped luminescent materials, such as low-pressure mercury (Hg), utilize europium (Eu^{3+}) and terbium (Tb^{3+}) and have been extensively explored for photon downconversion,[12−14] in which after the absorption of incident high-energy light beam, the materials can emit radiation with lower photon energies that can match to

*Address correspondence to yfchen@phys.ntu.edu.tw.

Received for review July 29, 2010 and accepted September 20, 2010.

Published online September 27, 2010.
10.1021/nn101817s

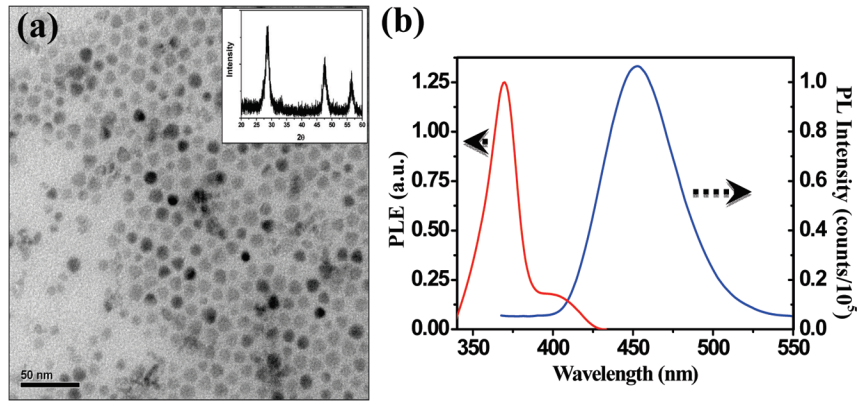

Figure 1. (a) TEM image of ZnS NPs. The averaged sizes of ZnS NPs are calculated to be 10 nm. XRD pattern of ZnS NPs with zinc blend structure (insets of upper corner). (b) PLE (left) and PL (right) spectra of ZnS NPs in toluene. The PLE spectrum was taken at the maximum of PL intensity (~450 nm). For the PL spectrum, the sample was excited by a light beam with 360 nm.

the bandgap of the active layer. Due to expansions of operating spectral range toward the ultraviolet, the downconverter materials can help in harvesting the full solar energy. However, up to now, this approach is not successful enough to be implemented into practical application.

II−VI semiconductor nanoparticles (NPs), known as quantum dots (QDs) materials are another good alternative of downconverter materials abundant in earth.[15] The reduced dimensionality of QDs exhibits quantization of their electronic energy levels, and consequently the blue-shift of optical absorption edge takes place. Because the QDs electronic energy levels and optical spectrum depend on their size, the effective bandgap can be tuned for the solar spectrum.[16] In addition, due to the low cost and easy fabrication, casting the group of II−VI semiconductor QDs films from colloidal methods has been explored for solar cells applications.[17] However, within the past years, environmental issues have aroused much attention in the world. Electrical product with heavy metal is controversial and prohibited from becoming available in the market. For instance, CdTe thin-film solar cell modules, not used on rooftops in city, are only installed in desert regions. In the group of II−VI semiconductor NPs, such as CdSe, CdTe, CdS, PbSe, and PbS, most of them contain the toxic elements of Cd, Pb, and Se. Fortunately, among all II−VI semiconductor NPs, ZnS is a promising candidates for PV applications because of its nontoxicity, low cost, high refraction index, and abundance in earth.[18]

In this work, we explore a strategy for improving monocrystalline Si-based solar cells by combining one-dimensional (1-D) Si nanotips and zero-dimensional (0-D) ZnS QDs together. Quite interestingly, it is found that the hybrid solar cell shows a large enhancement in the short-circuit current and the cell efficiency. Based on the spectral response and optical measurement, we demonstrate that ZnS QDs not only have the capability for frequency downconversion in ultraviolet region but also serve as antireflection coating for light trapping of incident light beam.

RESULTS AND DISCUSSION

Transmission electron microscopy (TEM) image of ZnS in Figure 1a shows that the NPs were uniform and well-dispersed on the TEM grid with an average

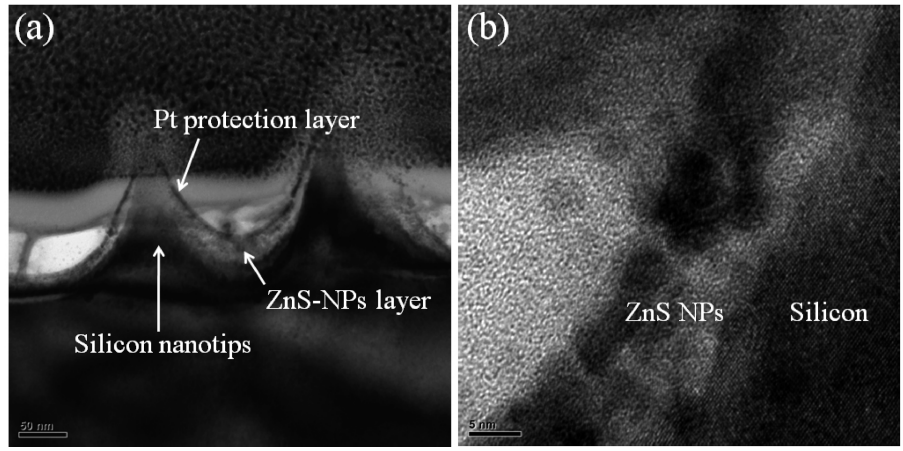

Figure 2. (a) A cross-sectional TEM image of the structure of Si nanotips after the integration of ZnS NPs. (b) High-resolution TEM image of the ZnS NPs/Si interface.

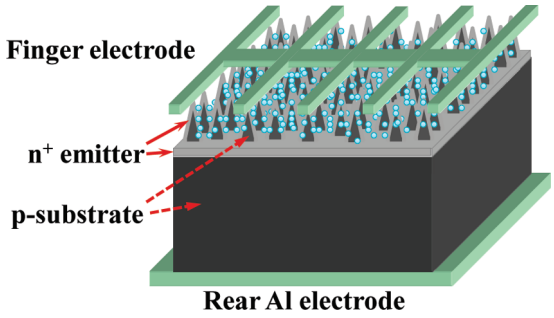

Figure 3. Schematic diagram of Si nanotips solar cell structure with ZnS NPs.

diameter of 10 nm. The X-ray diffraction (XRD) pattern of ZnS NPs is also shown in (insets of upper corner) the image. The peaks at 2θ values of 28.62, 47.84, and 56.63° can be indexed to the (111), (220), and (311) planes of ZnS, respectively, which match well with the standard diffraction data of ZnS zinc blend (JCPDS no. 01-0792). Figure 1b shows the excitation and fluorescence spectra of ZnS NPs in toluene. The fluorescence spectrum shows a peak at 450 nm excited by 360 nm. The broad peak is attributed to the trap-states emission of ZnS NPs.[18] Similar to the previous report,[19] the photoluminescence excitation spectrum (PLE) shows an excitation peak at around 370 nm and a shoulder band between 385 and 420 nm. It is evident that ZnS NPs exhibit frequency downconversion from ultraviolet to visible light (from ~370 to ~450 nm). This result will be discussed together with other optical measurement as shown below.

To examine experimental characterization on the real structure of the cell after the integration of ZnS NPs, the TEM samples were prepared using focus ion beam (FIB) techniques. As shown in Figure 2a, the cross-sectional details of Si nanotips array indicate that all nanotips are isolated, and the thickness of the ZnS layer is about 30 −50 nm (for the concentration of 6 mg/mL), depending on the position of Si nanotips. Besides, to prevent top-surface damage, a layer of platinum (Pt) deposited by a FIB instrument prior to the start of milling can also be observed on the top of ZnS layer. In Figure 2b, the TEM image taken near the edge of Si nanotips reveals the different physical properties between the QDs and the crystalline Si. A schematic of our structure configuration is shown in Figure 3.

Figure 4a shows the *I*−*V* characteristics of the Si nanotips solar cells with and without ZnS NPs. The comparison highlights the fact that 6 mg/mL ZnS NPs are effective in increasing the short-circuit current density from 18.9 to 22.7 mA/cm^2 and the power conversion efficiency from 6.57 to 7.20%. It is worth noting that open-circuit voltage (Voc) exhibits negligible change. This is because in principle the additional QDs do not change the Fermi energy distribution in the Si nanotips p−n junction. Another observation of the *I*−*V* characteristic obtained from the slope around the Voc indicates that, after integrating ZnS NPs on the solar cells, the fill factor declined slightly from 61 to 57.9%. It implies that ZnS NPs at the top side of the device will affect the conduction of electrons in the thin n$^+$ region toward the finger electrode, resulting in a bigger series resistance. Indeed, conduction phenomenon will be hampered due to electron trapping in ZnS, which is a wild bandgap system with a lot of trap states. Fortunately, a thin native insulating layer of SiO_2, most likely to be formed at the interface between the n$^+$ region and the ZnS NPs, provides an additional protection against these trap states. Thus, the improvement benefited from ZnS NPs is greatly larger than its fault. To further characterize the composite system, different concentrations of ZnS NPs were performed, as shown in Figure 4b. It helps us to find out the optimal concentration of ZnS NPs for power conversion efficiency.

In order to understand the underlying mechanism for the enhanced cell efficiency, we have performed the external quantum efficiency (EQE) measurement, in which a xenon light source is used as the illumination source. Figure 5a shows the EQE as a function of illumination wavelength for the solar cells with and without 6 mg/mL ZnS NPs, and Figure 5b shows the EQE enhancement factor between the devices with and without ZnS NPs. The introduction of ZnS NPs provides an enhanced quantum efficiency in the range from 350 to 1100 nm. According to the PLE and the fluorescence spectra of ZnS NPs shown in Figure 1b, the PLE takes place with the peak at ~370 nm, which is consistent with the position of the maximum

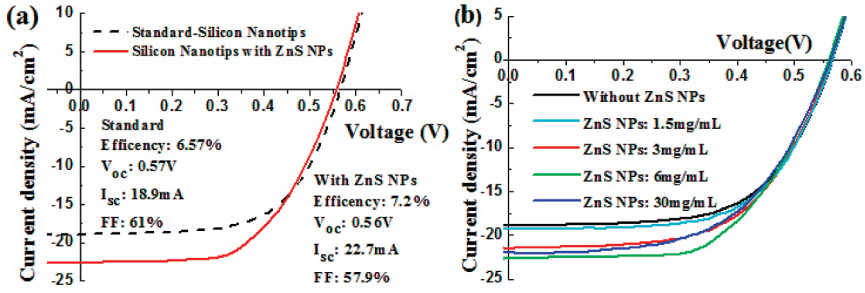

Figure 4. (a) Current density−voltage characteristics demonstrating the superior power conversion efficiency of the photovoltaic device spreading 6 mg/mL ZnS NPs as compared to the one without ZnS NPs (- - -) under AM1.5. (b) Current density−voltage characteristics with different concentration of ZnS NPs.

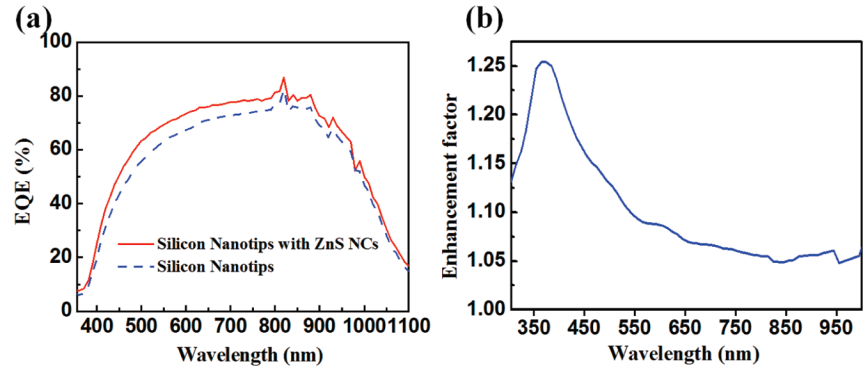

Figure 5. (a) EQE as a function of illumination wavelength for the Si nanotips solar cells with and without 6 mg/mL ZnS NPs showing the increased response due to the presence of ZnS NPs. (b) Enhancement in EQE indicating maximum enhancement monitored at ~400 nm wavelengths.

enhancement of EQE (~375 nm), as shown in Figure 5b. Therefore, the enhanced behavior of the spectral response below 425 nm can be attributed to the photon frequency downconversion. Since most of incident UV radiation produces electron−hole pairs near the device surface, the photogenerated carriers disappear easily through the recombination with surface defects, which can lead to inferior cell efficiency. However, with ZnS NPs on the front side, after photon downconversion, more photons are absorbed in the depletion region, and the photogenerated electron−hole pairs will be immediately separated by a built-in electric field, and the photovoltaic effect is enhanced.

For the spectral response above 425 nm, since there is no PLE signal from ZnS NPs, frequency downconversion cannot entirely account for the enhancement of EQE. To interpret the enhancement of EQE above 500 nm, let us recall the fact that, considering simple effective medium approximation of the NPs on the Si surface,[20] the average refractive index of the ZnS layer (n ~ 2.3), sandwiched between the refractive index of Si (n ~ 3.8) and air (n ~ 1), can act as an antireflection coating. To verify the effect of light trapping due to ZnS NPs, the reflectance spectrum is shown in Figure 6. We can see that ZnS NPs can reduce the reflectance covering the spectral range from 450 to 1100 nm. According to current density−voltage characteristics under AM1.5 (as shown in Figure 4b) and reflectance measurement (as shown in Figure 6) with various concentrations of ZnS NPs, the maximal efficiency, which coincides with the minimal reflectance, occurs at a specific concentration (6 mg/mL) of ZnS. This behavior can be easily understood according to the average refractive index of the ZnS−air layer serving as an optimal antireflection layer. It should be noted that, since Si is a poor absorber due to the nature of its indirect bandgap, light trapping resulting from antireflection coating is especially important at long wavelengths (close to the bandgap) in Si solar cells. For the large area fabrication, Si nitride antireflection coating, deposited by plasma enhanced chemical vapor deposition (PECVD),[8,9] has normally been used in the field of Si solar cell, but it is still a costlier one. The creation of a suitable colloidal NPs ink for use in the large area process is a potential step in the development of low-cost antireflection coating. ZnS QDs, being a wide bandgap semiconductor with high refractive index and high transmittance in visible regions, are another good choice to attain low cost and easy fabrication and to be environmentally friendly, in addition to the novel property of photon downconversion shown in the current report. In addition, the surface roughness of Si is increased after integrating ZnS NPs and reduces sensitivity on incidence light angles. As a result, photons that reach the ZnS−air interface have more chance of being trapped in the solar cell and then being converted to photocurrents, especially at dawn and sunset (large incident angle).[21] This result provides another advantage because the Si solar cell has inferior average-generated electricity (due to less working time). With rough morphology, solar cell modules are not necessarily setting up a tracking system to maintain a normal incidence of light beams, which needs additional power consumption and complication in PV systems.[21] According to the discussion above, the origin of enhanced short-circuit photocurrent in hybrid ZnS NPs and Si nanotips solar cells therefore can

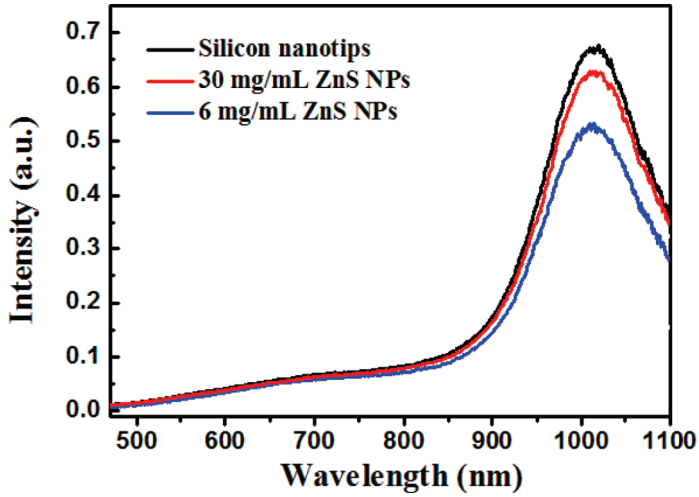

Figure 6. Reflectance of Si nanotips solar cells with various concentration of ZnS NPs (0, 6, and 30 mg/mL).

be attributed to both effects of frequency downconversion and light trapping.

To further characterize the possible systems, several complementary experiments have been performed. We have attempted PbS and CdSe QDs, but the results are not as good as that of ZnS QDs embedded in Si nanotips solar cells. It is possible that PbS QDs are intrinsic p-type materials[22] and thus form an opposite direction of p−n junction to the original one. The structure of p−n−p multijunctions leads to inferior cell efficiency. For the case of CdSe QDs, unlike UV absorption of ZnS QDs, the absorption spectrum of CdSe QDs extends to the visible region.[23] However, visible light can produce electron−hole pairs in the depletion region, which can efficiently be used by Si solar cells *via* a built-in electric field. The CdSe QDs on top of the cell absorb and diminish the numbers of visible photons, and thus the enhancement is less than ZnS QDs even though they have a good quantum yield.

CONCLUSIONS

In summary, ZnS nanoparticles (NPs) and Si-nanotips have been integrated to form nanocomposite solar cells. We have shown that the hybrid system can significantly enhance power conversion efficiency under AM1.5 illumination. The underlying mechanism of the enhancement can be attributed to frequency downconversion as well as light trapping. We believe that this approach may find promising applications in Si-based solar cells and opens a new possible scheme to exploiting semiconductor NPs for energy devices.

METHODS

Quantum Dots Synthesis. The ZnS NPs were prepared by wet solution phase chemical syntheses with some modifications. In brief, 272 mg of $ZnCl_2$, 10 mL of oleylamine, and 2.3 g of trioctylphosphine oxide were mixed and then reacted under N_2 gas at 170 °C for 1 h to form the Zn−oleylamine complex. Afterward, 2.5 mL oleylamine solution of sulfur (96 mg) was quickly injected into the solution. The resulting solution was heated to 320 °C and kept for 1 h. After the solution was cooled to room temperature, a large amount of ethanol was added to precipitate ZnS NPs followed by centrifugation. The solid product was dispersed very well in toluene.

Device Fabrication. P-type, (100)-oriented Si wafers with resistivity in the range 7−12 Ω cm were used as substrates. The thickness of wafers was about 550 μm. The surfaces of wafers were first cleaned to eliminate any metal impurities and anything organic. Initially, a 10 nm silver (Ag) layer was deposited on substrates using a sputtering system. After 10 min of thermal annealing in a furnace at 550 °C, we exploit-assembled Ag NPs as a mask for reactive ion etching (RIE) to fabricate Si nanotips. The parameters used in this step were a flow of 100 sccm of CF_4, a RF power of 100W, and an etching time of 30 min. Ag particles at the tips can be removed by nitric acid.

To investigate the effect of ZnS NPs on Si-based solar cells, the solar cells were fabricated by a conventional solar cell process. In brief, this process includes standard RCA cleaning, phosphorus coating on the textured front side, thermal diffusion of phosphorus by rapid thermal process (RTP) at 850 °C for 4 min, and phosphosilicate glass (PSG) layers removal by dipping them in BOE solution for 2 min. After each fabrication step, the solar cell was cut into 1.5 × 1.5 cm pieces to measure electrical and optical characteristics.

In order to estimate the influence of different concentrations of ZnS NPs quantitatively, we spread a fixed volume of the colloid (120 μL) on solar cells. Toluene was dried quickly. Every measurement, such as current−voltage and external quantum efficiency and reflection, was done before and after an incremental increase. To verify the reproducibility, the device was immersed in toluene to clean the colloid after each measurement, and the above-mentioned procedure was repeated again.

Characterization. The current−voltage characteristics of the solar cells were illuminated under AM1.5G, which was provided by an ORIEL class A solar simulator (100 mW/cm^2) and measured using a Keithley 236 sourcemeter. The light intensity of measurement system was calibrated by NREL reference cell. For the external quantum efficiency spectrum measurements, the incident light was generated by Xenon light source, chopped at 100 Hz, and dispersed by a monochromator. The light intensity was calibrated using a commercial Si photodetector (for wavelength of 300−1100 nm), and the photocurrent under short-circuit condition was detected by a lock-in amplifier. A UV−vis-NIR spectrophotometer with standard mirror optics was used to measure the specular reflectance in the 500−1100 nm range at an incidence angle of 10°. The phase and the crystallographic structure of ZnS NPs were characterized by powder X-ray diffraction (PXRD) using a bruker D8 tool diffractometer and TEM (Philips Technai G2). The photoluminescense spectra (PL) of ZnS NPs were obtained by measuring the transmittance of the films on transparent glass substrates, using a pulsed diode laser with 325 nm wavelength as the excitation source. The PL spectra were recorded by a Triax 320 monochromator and detected by a photomultiplier tube (PMT). For the photoluminescence excitation (PLE) measurement, a Xe lamp and Spectra Pro 300i monochromator were used as the excitation source. To locate a specific feature on our device, TEM samples are prepared using focus ion beam (FIB) techniques. The area of Si nanotips is identified by SEM, and trenches were milled to leave a thin wall of Si. Platinum (Pt) is deposited by commercially available machines to serve as a protection layer. To properly use TEM (FEI Tecnai G2 F-20), the trimming process continues until the remaining wall is thin enough for electron transparent (~100 nm).

Acknowledgment. This work was supported by the National Science Council and the Ministry of Education of the Republic of China. We thank Yu-Feng Ko (TEM Department Manager) from MA-TEK Inc. for providing the FIB technique and HRTEM image supports.

REFERENCES AND NOTES

1. Green, M. A. *Solar cells: Operating Principles, Technology and System Applications*; The University of New South Wales: Sydney, Australia, 1998.
2. Green, M. A. *Silicon Solar cells: Advanced Principles and Practice*; The University of New South Wales: Sydney, Australia, 1995.
3. Nelson, J. *The Physics of Solar Cells*; Imperial College Press: London, 2003.
4. Würfel, P. *Physics of Solar Cells*; Wiley-VCH Verlag GmbH & Co. HGaA: Weinheim, Germany, 2003.
5. Peng, K.; Wang, X.; Lee, S. T. Silicon Nanowire Array Photoelectronchemical Solar Cells. *Appl. Phys. Lett.* **2008**, *92*, 163103.
6. Stelzner, T.; Pietsch, M.; Andrä, G.; Falk, F.; Ose, E.; Christianse, S. Silicon Nanowires-Based Solar Cells. *Nanotechnology* **2008**, *19*, 295203.
7. Martinet, C.; Paillard, V.; Gagnaire, A.; Joseph, J. Deposition of SiO_2 and TiO_2 Thin Films by Plasma Enhanced Chemical Vapor Deposition for Antireflection Coating. *J. Non-Cryst. Solids* **1997**, *216*, 77–82.

8. Hezel, R.; Schörner, R. Plasma Si nitride - A Promising Dielectric to Achieve High Quality Silicon MIS/IL Solar Cells. *J. Appl. Phys.* **1981**, *52*, 3076–3079.
9. Singh, P.; Shivaprasad, S. M.; Lal, M.; Husain, M. Angle-Dependent XPS Analysis of Silicon Nitride Film Deposited on Screen-Printed Crystalline Silicon Solar Cell. *Sol. Energy Mater. Sol. Cells* **2009**, *93*, 19–24.
10. Lee, S. E.; Choi, S. W.; Yi, J. Double-Layer Anti-Reflection Coating Using MgF_2 and CeO_2 Films on a Crystalline Silicon Substrate. *Thin Solid Films* **2000**, *376*, 208–213.
11. Aroutiounian, V. M.; Maroutyan, K. R.; Zatikyan, A. L.; Touryan, K. J. Calculations of The Reflectance of Porous Silicon and Other Antireflection Coating to Silicon Solar Cells. *Thin Solid Films* **2002**, *403*, 517–521.
12. Richards, B. S. Luminescent Layers for Enhanced Silicon Solar Cell Performance: Down-Conversion. *Sol. Energy Mater. Sol. Cells* **2006**, *90*, 1189–1207.
13. Aarts, L.; van der Ende, B. M.; Meijerink, A. Downconversion for Solar Cells in NaYF4: Er, Yb. *J. Appl. Phys.* **2009**, *106*, 023522.
14. Wegh, R. T.; Donker, H.; van Loef, E. V. D.; Oskam, K. D.; Meijerink, A. Quantum Cutting through Downconversion in Rare-Earth Compounds. *J. Lumin.* **2000**, *87*, 1017–1019.
15. Kaplan, A.; Sajwani, A.; Li, Z. Y.; Palmer, R. E. Efficient Vacuum Ultraviolet Light Frequency Downconversion by Thin Films of CdSe Quantum Dots. *Appl. Phys. Lett.* **2006**, *88*, 171105.
16. Norris, D. J.; Bawendi, M. G. Measurement and Assignment of The Size-Dependent Optical Spectrum in CdSe Quantum Dots. *Phys. Rev. B: Condens. Matter Mater. Phys.* **1996**, *53*, 16338–16346.
17. Gur, I.; Fromer, N. A.; Geier, M. L.; Alivisatos, A. P. Air-Stable All-Inorganic Nanocrystal Solar Cells Processed from Solution. *Science* **2005**, *310*, 462–465.
18. Zhao, Y.; Zhang, Y.; Zhu, H.; Hadjipanayis, G. C.; Xiao, J. Q. Low-Temperature Synthesis of Hexagonal (Wurtzite) ZnS Nanocrystals. *J. Am. Chem. Soc.* **2004**, *126*, 6874–6875.
19. Manam, J.; Chatterjee, V.; Das, S.; Choubey, A.; Sharma, S. K. Preparation, Characterization and Study of Optical Properties of ZnS Nanophosphor. *J. Lumin.* **2010**, *130*, 292–297.
20. Rowlands, S. F.; Livingstone, J.; Lund, C. P. Optical Modelling of Thin Film Solar Cells with Textured Interfaces Using The Effective Medium Approximation. *Sol. Energy* **2004**, *76*, 301–307.
21. Chen, C. P.; Lin, P. H.; Chen, L. Y.; Ke, M. Y.; Cheng, Y. W.; Huang, J. J. Nanoparticle-Coated N-ZnO/p-Si Photodiodes with Improved Photoresponsivities and Acceptance Angles for Potential Solar Cell Applications. *Nanotechnology* **2009**, *20*, 245204.
22. Zarghami, M. H.; Liu, Y.; Gibbs, M.; Gebremichael, E.; Webster, C.; Law, M. P-Type PbSe and PbS Quantum Dot Solids Prepared with Short-Chain Acids and Diacids. *ACS Nano* **2010**, *4*, 2475–2485.
23. Sun, B.; Findikoglu, A. T.; Sykora, M.; Werder, D. J.; Klimov, V. I. Hybrid Photovoltaics Based on Semiconductor Nanocrystals and Amorphous Silicon. *Nano Lett.* **2009**, *9*, 1235–1241.